

aliphatic diols in the presence of 0.2 mol% of $\text{HfCl}_4 \cdot (\text{THF})_2$ in *o*-xylene with the removal of water for 1 day (28, 29). In most cases, polycondensation proceeded quantitatively (Table 3). Although no polycondensation of aromatic dicarboxylic acids and aromatic diols occurred because of the insolubility of aromatic carboxylic acids for *o*-xylene and less nucleophilicity of aromatic diols, the polycondensation to semiaromatic polyesters successfully proceeded.

In direct esterification, the catalytic use of inorganic salts is quite practical because of its simplicity and applicability to large-scale operations. Hafnium(IV) salts, which are hydrolytically more stable than Ti(IV) salts, are extremely active catalysts for direct esterification and polycondensation to polyesters. This catalytic system should be useful as an environmentally and industrially ideal condensation in the near future.

References and Notes

- P. T. Anastas, J. C. Warner, *Green Chemistry: Theory and Practice* (Oxford Univ. Press, Oxford, 1998).
- R. C. Larock, *Comprehensive Organic Transformations* (VCH, New York, 1989), p. 966.
- G. A. Olah, T. Keumi, D. Meidar, *Synthesis* **1978**, 929 (1978).
- Y. Masaki, N. Tanaka, T. Miura, *Chem. Lett.* **1997**, 55 (1997).
- Y. Izumi, K. Urabe, *Chem. Lett.* **1981**, 663 (1981).
- P. K. Kadaba, *Synthesis* **1972**, 628 (1972).
- W. W. Lawrance Jr., *Tetrahedron Lett.* **12**, 3453 (1971).
- E. C. Blossley, L. M. Turner, D. C. Neckers, *Tetrahedron Lett.* **14**, 1823 (1973).
- R. Nakao, K. Oka, T. Fukumoto, *Bull. Chem. Soc. Jpn.* **54**, 1267 (1981).
- K. Tanabe, H. Hattori, Y. Ban'i, A. Mitsutani, Japanese Patent 55-115570 (1980).
- J. F. White, Japanese Patent 52-75684 (1977).
- K. Steliou, A. Szczygielska-Nowosielska, A. Favre, M. A. Poupard, S. Hanessian, *J. Am. Chem. Soc.* **102**, 7578 (1980).
- A. K. Kmar, T. K. Chattopadhyay, *Tetrahedron Lett.* **28**, 3713 (1987).
- J. Otera, N. Dan-oh, H. Nozaki, *J. Org. Chem.* **56**, 5307 (1991).
- M. Hino, K. Arata, *Chem. Lett.* **1981**, 1671 (1981).
- K. Takahashi, M. Shibagaki, H. Matsushita, *Bull. Chem. Soc. Jpn.* **62**, 2353 (1989).
- Z. Chen, T. Iizuka, K. Tanabe, *Chem. Lett.* **1984**, 1085 (1984).
- T. Ogawa, T. Hikasa, T. Ikegami, N. Ono, H. Suzuki, *J. Chem. Soc. Perkin Trans. 1* **1994**, 3473 (1994).
- K. Suzuki, *Pure Appl. Chem.* **66**, 1557 (1994).
- I. Hachiya, M. Moriwaki, S. Kobayashi, *Bull. Chem. Soc. Jpn.* **68**, 2053 (1995).
- S. Kobayashi, M. Moriwaki, H. Hachiya, *Bull. Chem. Soc. Jpn.* **70**, 267 (1997).
- K. Ishihara, S. Ohara, H. Yamamoto, *J. Org. Chem.* **61**, 4196 (1996).
- K. Ishihara, S. Ohara, H. Yamamoto, *Macromolecules* **33**, 3511 (2000).
- The model reaction in Table 1 that uses $\text{Sc}(\text{OTf})_3$ as a catalyst gave α -tetralone as a major product.
- K. Ishihara, M. Kubota, H. Kurihara, H. Yamamoto, *J. Org. Chem.* **61**, 4560 (1996).
- K. Ishihara, M. Kubota, H. Yamamoto, *Synlett* **1996**, 265 (1996).
- J. Otton et al., *J. Polym. Sci. Part A Polym. Chem.* **26**, 2199 (1988).
- S. R. Sandler, W. Karo, *Polymer Synthesis* (Academic Press, San Diego, CA, ed. 2, 1992), vol. 1, chap. 2.
- The typical procedure of polycondensation is as follows. A flame-dried, 5-ml, single-necked, round-bottomed flask that is equipped with a Teflon-coated magnetic stirring bar and a 5-ml pressure-equalized addition funnel [containing a cotton plug and 4 Å molecular sieves (~1.5 g)] surmounted by a reflux condenser was charged with α,ω -hydroxycarboxylic acid (10 mmol) or α,ω -dicarboxylic acid (10.0 mmol) and α,ω -diol (10.0 mmol) as substrates and $\text{HfCl}_4 \cdot (\text{THF})_2$ (0.200 mmol) as a catalyst in *o*-xylene (2 ml). The mixture was brought to reflux with the removal of water. After 1 day, the resulting mixture was cooled to ambient temperature, dissolved with chloroform, and precipitated with acetone or methanol to furnish pure polyester as a white solid in quantitative yield.
- Web table 1, a more extensive version of Table 2, is available at www.sciencemag.org/feature/data/1054771.shl.

9 August 2000; accepted 26 September 2000

Solar Wind Record on the Moon: Deciphering Presolar from Planetary Nitrogen

Ko Hashizume,^{1,2*} Marc Chaussidon,¹ Bernard Marty,^{1,3} François Robert⁴

Ion microprobe analyses show that solar wind nitrogen associated with solar wind hydrogen implanted in the first tens of nanometers of lunar regolith grains is depleted in ^{15}N by at least 24% relative to terrestrial atmosphere, whereas a nonsolar component associated with deuterium-rich hydrogen, detected in silicon-bearing coatings at the surface of some ilmenite grains, is enriched in ^{15}N . Systematic enrichment of ^{15}N in terrestrial planets and bulk meteorites relative to the protosolar gas cannot be explained by isotopic fractionation in nebular or planetary environments but requires the contribution of ^{15}N -rich compounds to the total nitrogen in planetary materials. Most of these compounds are possibly of an interstellar origin and never equilibrated with the ^{15}N -depleted protosolar nebula.

Solar system objects such as terrestrial planets, meteorites, and interplanetary dust particles (IDPs) exhibit up to a factor of 3 variation in their $^{15}\text{N}/^{14}\text{N}$ ratios [see, e.g. (1–7)]. These variations may reflect the heterogeneous distribution of isotopically distinct N components in the protosolar nebula. However the N isotopic composition of the sun, a potential reference for the nebular composition, is still unknown. The lunar regolith, irradiated by the solar wind (SW) and solar energetic particles (SEPs), contains information on the elemental and isotopic abundances of volatile elements in the SW and the sun.

Rare gas studies (8–11) have shown that the lunar regolith records the history of SW irradiation of the moon. In the case of N, however, the SW component has not been identified because of several contrasting interpretations of the 30% variability in the N isotopic composition found in lunar regoliths. One interpretation attributes the variation to

secular variation of the isotopic composition of the SW (8–10). Lunar samples that are considered to have been irradiated >1 billion years ago (Ga) tend to be depleted in ^{15}N relative to samples that were exposed more recently. Alternatively, the variation could be due to a mixture in different proportions of solar and nonsolar N sources, such as meteorites, comets, or the fractionated terrestrial atmosphere (12–14). This interpretation is supported by 3- to 10-fold excesses of N relative to the SW heavy rare gases in lunar regolith samples.

Because SW-derived isotopes are implanted at shallow depths, characteristic of SW ion energies (15), knowledge of the distribution of N isotopes in the surface layers of lunar regolith grains should explain the nature of surface-correlated N components. We used further improvements of the shallow-depth profiling technique, developed for the extraction of SW Li from bulk lunar regolith samples (16), to characterize with a depth resolution of 10 nm the isotopic composition of N sitting in individual lunar grains (17). Relatively large mineral grains, 500- to 1000- μm -sized ilmenite, pyroxene, or olivine, from two Apollo 17 samples (79035 and 71501) have been analyzed. The 79035 breccia is thought to have been irradiated by the SW at 1 to 2 Ga, whereas the 71501 soil is thought to have been irradiated at 100 million years ago (Ma) (11). Previous analyses by conventional methods have shown that the

¹Centre de Recherches Pétrographiques et Géochimiques-CNRS, BP 20, 54501 Vandoeuvre-lès-Nancy Cedex, France. ²Department of Earth and Space Sciences, Graduate School of Sciences, Osaka University, Toyonaka, Osaka 560-0043, Japan. ³Ecole Nationale Supérieure de Géologie-INPL, rue de doyen Marcel Roubault, BP 40, 54501 Vandoeuvre-lès-nancy Cedex, France. ⁴Laboratoire de Minéralogie, Muséum National d'Histoire Naturelle-CNRS, 61 rue Buffon, 75005 Paris, France.

*To whom correspondence should be addressed. E-mail: kohash@ess.sci.osaka-u.ac.jp

REPORTS

$\delta^{15}\text{N}$ ranges between -200 and $+39\%$ (where $\delta^{15}\text{N}$ stands for the per mil deviation of the $^{15}\text{N}/^{14}\text{N}$ ratio relative to terrestrial atmospheric N having $^{15}\text{N}/^{14}\text{N} = 0.00368$) in sample 79035 and between -22 and $+73\%$ in sample 71501 (9, 10).

Contrasting distributions of N isotopes with depth have been observed in different grains of the two lunar regolith samples (Fig. 1) (18). In sample 79035, $\delta^{15}\text{N}$ values as low as -240% were observed for depths <120 nm, whereas $\delta^{15}\text{N}$ values up to $+50\%$ were present in the first ~ 50 nm of the surface of grains in sample 71501. N concentrations decrease with depth from several thousands or hundreds of parts per million (ppm) at the surface down to ~ 100 ppm at ~ 150 -nm depth in the grains, which is thought to partly represent the analytical blank (19). At greater depth, no systematic differences in the $\delta^{15}\text{N}$ values are observed between the two samples. They range between -100 and $+50\%$, although their large error bars (18) make $\sim 95\%$ of the data difficult to discriminate from the blank value. Differences in the H isotopic ratios are observed between the two sets of samples. Grains in sample 79035 have δD values down to -950% , indicating the presence of pure SW H, whereas enrichments of D by as much as $+600\%$ (i.e., typical of nonsolar H) are present in sample 71501. Part of this D enrichment may result from in situ spallation, but even after correction for such a contribution (20), the occurrence of D implanted together with H [$\delta\text{D}_{\text{trapped}} = +470\%$ (18)] highlights the contribution of a nonsolar H component. In addition, a surface coating containing several thousand ppm of Si is observed on ilmenite grains from sample 71501 having positive $\delta^{15}\text{N}$ values.

The depth profiling data indicate that SW N is characterized by a depletion of ^{15}N relative to terrestrial N, such as in sample 79035, with $\delta^{15}\text{N}$ values of -240% or lower (21), for two main reasons. First, the light N component in sample 79035 is distributed within the first 100 nm, with $>80\%$ residing within the 50-nm-thick surface layer (Fig. 1B, open squares with crosses inside), which is a typical depth for SW implantation. Second, the isotopically light N component ($\delta^{15}\text{N} \leq -240\%$) is associated with D-free H characteristic of the SW (Figs. 1 and 2). This component shows a $\text{N}_{\text{light}}/\text{H}_{\text{solar}}$ ratio that is 500 times the solar ratio that we attribute to the higher diffusivity of H relative to N, in agreement with (i) the smooth, bell-shaped profile of the H concentration in sample 79035, indicative of volume diffusion (Fig. 1B), and (ii) $^{36}\text{Ar}/^4\text{He}$ ratios that are 100 times the solar ratio interpreted as resulting from diffusional loss of He (22). Furthermore, the origin of the heavy N component in sample 71501 is most likely nonsolar (i) because it is associated with a Si-rich layer

observed at the ilmenite surface (Fig. 1D) and (ii) because the corresponding $\delta^{15}\text{N}$ and δD values are close to chondritic values such as those of the CI chondrites (1). In sample 71501, the depth at which a H spike is observed

(e.g., ~ 150 nm in Fig. 1D) possibly corresponds to the surface of the grain before the Si, ^{15}N -rich, and D-bearing coat was acquired during the process of regolith gardening. Similar coatings were observed by a

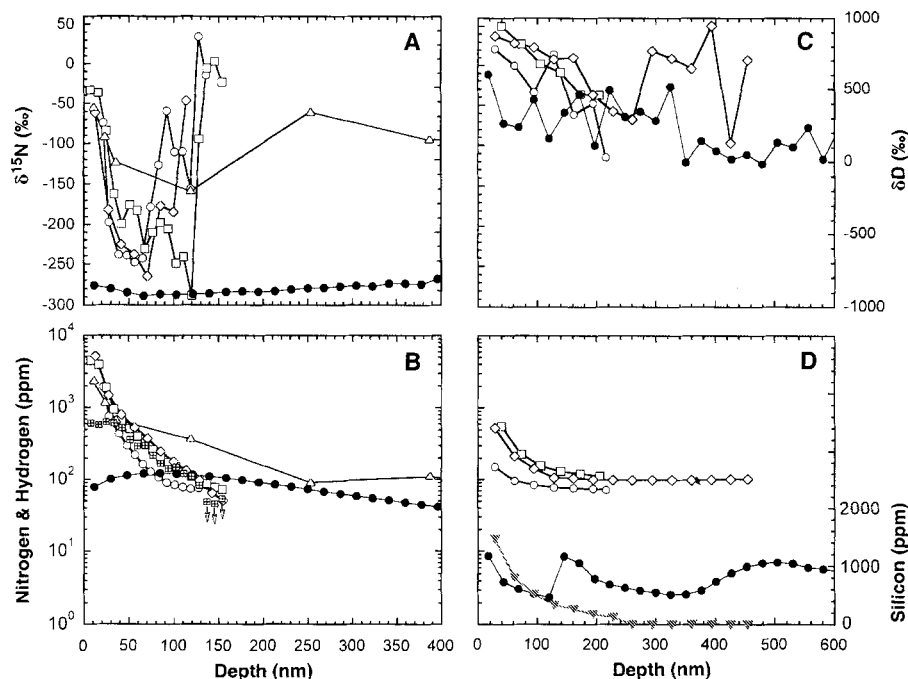
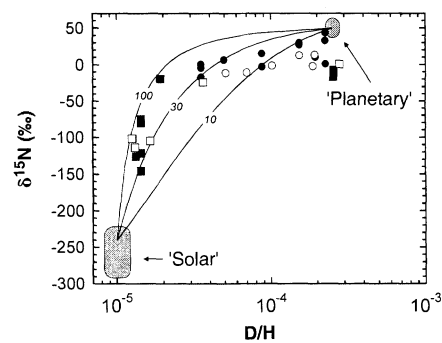


Fig. 1. Examples of variations with depth of $\delta^{15}\text{N}$ and δD values and N, H, and Si concentrations in a grain each from two lunar soil samples, 79035 and 71501 (18). N depth profiles (open symbols) are shown (A and B) at four different locations on one silicate grain (grain 1) of sample 79035 and (C and D) for three different locations on one ilmenite grain (grain A) of sample 71501. One H depth profile (solid circles) has been measured in ilmenite from sample 71501, and the Si depth profile [shaded triangles in (D)] was determined in ilmenite from sample 71501. N data are corrected for the blank value [~ 100 ppm N and $\delta^{15}\text{N} = -15 \pm 15\%$ (19)]. The variation with depth of the concentration of light N (i.e., SW N) in sample 79035 ($\delta^{15}\text{N} = -240\%$), computed by assuming a binary mixing with N having $\delta^{15}\text{N} = 0\%$, is shown in (B) by open squares with crosses inside. The arrows in (B) indicate upper limits of the SW N concentrations.

Fig. 2. Mean $\delta^{15}\text{N}$ values versus mean D/H ratios for all analyzed grains, five grains for sample 79035 and six grains for sample 71501 (18), including the two grains plotted in Fig. 1. (Numbers of analytical points differ from the numbers of grains because analyses were duplicated for some grains.) The data for samples 79035 and 71501 are plotted in squares and circles, respectively. Solid symbols represent mean values taken from the depth profile at <100 -nm depth. Open symbols represent mean values for the entire depth profile (34). Three mixing curves are plotted with different elemental abundance ratios assumed for the end-members ("solar" and "planetary"). The "solar" isotopic ratios are taken from the lowest ratios observed in grain 1 from sample 79035, whereas the "planetary" values are from the highest ratios in grain A from sample 71501. Numbers given for the respective curves are the elemental abundance ratios [i.e., $(\text{N}/\text{H})_{\text{p}}/(\text{N}/\text{H})_{\text{s}}$]. The only adjustable parameter to draw a unique mixing curve connecting two end-members with fixed isotopic ratios is the elemental abundance ratio. (Therefore, the mixing curve holds even when H is partly lost from the grain by later events such as heating of grains, as far as the H of the two end-members is lost proportionally.) The mixing curve best fits the observed values when the N/H ratio for the planetary component is assumed to be ~ 30 times the solar value, consistent with the proportion of the N/H ratios (10 to 45), comparing the D-rich grain A from sample 71501 and the solar gas-rich grains, such as grain 1 from sample 79035. Deviation of respective data from the curve can be due to the contribution of contamination N or the production of cosmogenic D. The population of data at a $\delta^{15}\text{N}$ range of 0 to -30% may be partly due to such a N contamination effect.



transmission electron microprobe in lunar soil grains and were attributed to the contribution of planetary material impacting on the moon (23). The presence of nonsolar components in sample 71501 is further evidenced by the heterogeneous distribution of N and C; high $\delta^{15}\text{N}$ values of +130‰ and high $\delta^{13}\text{C}$ values of +60‰ were found at the surface of a 500- μm -sized grain from sample 71501 (grain G) only in a 50-nm-thick layer of a localized area of 50 μm by 50 μm , whereas $\delta^{15}\text{N}$ and $\delta^{13}\text{C}$ values for the other part of the grain were within the blank range (which is generally lower than -10‰ for $\delta^{13}\text{C}$).

The low $\delta^{15}\text{N}$ SW component identified in sample 79035 is also present, but is less prominent, in most of the grains from sample 71501, in agreement with a bulk SW Xe abundance in sample 71501 (9) that is, at most, one-third that in sample 79035 (10). D/H ratios and $\delta^{15}\text{N}$ values for both samples can be plotted along mixing curves between two end-members defined by the SW component (D free and ^{15}N depleted) observed in sample 79035 and the surface coating of sample 71501 grain A (Fig. 2). About 80% of the surface-correlated N in grains from sample 71501 is attributable to a nonsolar component, which masks the N isotopic signature of the SW component at shallow

depth (<100 nm). The light N component in sample 71501 can be identified at a greater depth (≥ 200 nm) but only with a minimum $\delta^{15}\text{N}$ value of -100‰ (Fig. 1C). The $\delta^{15}\text{N}$ value is the same as the one previously proposed for SEPs (8), which is implanted to a greater depth than the SW component. Furthermore, comparison with Ne [$^{20}\text{Ne}/^{22}\text{Ne}$ value for the SEP is 23% lower than that of the SW (24)] suggests a $\delta^{15}\text{N}$ value for SEP around -120‰ for a SW $\delta^{15}\text{N}$ value of -240‰, assuming that the heavier isotopic composition of SEP-Ne is due to a fractionation process in an ion acceleration mechanism in solar flare events following a constant power of mass (m^{α}) law. A detailed model study (25), although involving a process with different mass dependence (i.e., a resonance process), gives a consistent result for the fractionation degree of SEP-N.

A substantial contribution of the nonsolar N to the lunar regolith provides a possible explanation for its systematically higher bulk N/rare gas (e.g., ^{36}Ar) ratios relative to the solar ratio (9, 10, 12-14). However, high N/ ^{36}Ar cannot be attributed only to nonsolar components because single grains in sample 79035 with $\delta^{15}\text{N}$ values as low as -240‰ have N/ ^{36}Ar ratios that are still about four to five times the solar ratio (14). Such high N/rare gas ratios could result from a preferential retention of N relative to rare gases in silicates under the lunar reducing environment (26). For sample 79035, the required loss of Ar is limited to 70 to 80%, considering that the N/Ar ratio of the SW might be 20 to 30% as high as the solar ratio (27).

Recently, two spacecraft measurements yielded contrasting $\delta^{15}\text{N}$ values of $+360^{+520}_{-290}\text{‰}$ for the present-day SW [Solar and Heliospheric Observatory (SOHO)] (28) and $-480^{+240}_{-280}\text{‰}$ for ammonia in the jovian atmosphere (Infrared Space Observatory-Short Wavelength Spectrometer) (29). The SOHO measurement is not consistent with our $\delta^{15}\text{N}$ value of less than or equal to -240‰ for the SW. However, the range reported for ammonia in Jupiter's atmosphere strongly suggests a negative $\delta^{15}\text{N}$ value for the protosolar nebula, in agreement with our present SW measurement. Solid planetary objects, including terrestrial planets, meteorites, and IDPs, all have $\delta^{15}\text{N}$ values higher than the solar value derived from lunar soil (Fig. 3). This gap could be explained by the incorporation of various nucleosynthetic components into planetary objects or by ^{15}N enrichment through isotopic fractionation. Although some of circumstellar grains in primitive meteorites contain anomalous N (30), they cannot contribute to filling the gap between the solar and the planetary $\delta^{15}\text{N}$ range because their abundances are low and most of them are enriched in ^{14}N . While there are several prominent cases where isotopic fractionation by physical (i.e., mass-transfer) processes might take place [e.g., ion acceleration mechanism for

SEPs (24, 25) or hydrodynamic escape for the martian atmosphere (31)], it is difficult to explain the entire $\delta^{15}\text{N}$ variation in the solar system by these processes (32). The only process that may explain the whole gap is isotopic fractionation by chemical reactions of the order of 10 K (33). Most planetary N may have been derived from presolar solids fractionated by interstellar chemistry, like organic matter observed in IDPs (7). Systematic enrichment of ^{15}N in planetary material may reflect a nebular environment where the interstellar matter was never isotopically equilibrated with the ^{15}N -depleted nebular gas.

References and Notes

1. J. F. Kerridge, *Geochim. Cosmochim. Acta* **49**, 1707 (1985).
2. M. M. Grady, I. P. Wright, L. P. Carr, C. T. Pillinger, *Geochim. Cosmochim. Acta* **50**, 2799 (1986).
3. N. Sugiura, K. Hashizume, *Earth Planet. Sci. Lett.* **111**, 441 (1992).
4. C. A. Prombo, R. N. Clayton, *Geochim. Cosmochim. Acta* **57**, 3749 (1993).
5. M. M. Grady, C. T. Pillinger, *Earth Planet. Sci. Lett.* **116**, 165 (1993).
6. K. Hashizume, N. Sugiura, *Geochim. Cosmochim. Acta* **59**, 4057 (1995).
7. S. Messenger, R. M. Walker, *AIP Conf. Proc.* **402**, 545 (1997).
8. J. F. Kerridge, *Rev. Geophys.* **31**, 423 (1993).
9. U. Frick, R. H. Becker, R. O. Pepin, *Proc. Lunar Planet Sci. Conf. XVIII*, 87 (1988).
10. R. H. Becker, R. O. Pepin, *Geochim. Cosmochim. Acta* **53**, 1135 (1989).
11. R. Wieler, K. Kehm, A. P. Meshik, C. M. Hohenberg, *Nature* **384**, 46 (1996).
12. J. Geiss, P. Bochsler, in *The Sun in Time*, C. P. Sonett, M. S. Giampapa, M. S. Matthews, Eds. (Univ. of Arizona Press, Tucson, 1991), pp. 98-117.
13. R. Wieler, F. Humbert, B. Marty, *Earth Planet. Sci. Lett.* **167**, 47 (1999).
14. K. Hashizume, B. Marty, R. Wieler, *Lunar Planet. Sci. XXX*, abstract 1567 (1999) [CD-ROM].
15. J. F. Ziegler, J. P. Biersack, U. Littmark, *The Stopping and Ranges of Ions in Matter* (Pergamon, New York, 1985), vol. 1.
16. M. Chaussidon, F. Robert, *Nature* **402**, 270 (1999).
17. Ion probe analyses were performed at Centre de Recherches Pétrographiques et Géochimiques (CRPG)-CNRS (Nancy, France) with the Cameca ims-1270. Relatively flat surfaces of unpolished mineral grains embedded in In were sputtered by a (14 keV, 1 to 3 nA) primary Cs⁺ beam using electron flooding. The primary beam was rastered over 50 by 50 to 100 by 100 μm^2 , using dynamic transfer to insure high-enough transmission with a depth resolution of 10 nm. H analyses and C, N, and Si analyses were performed separately. Secondary ions of H⁻, CC⁻, and CN⁻, and their isotopes, accelerated to 10 keV, were measured in monocollection by using an electron multiplier. A mass resolution power ($M/\Delta M$) of >7500 was required to resolve $^{11}\text{B}^{16}\text{O}^-$ from $^{12}\text{C}^{15}\text{N}^-$. We used a mid-ocean ridge basalt glass (East Pacific Rise, 12°50'N CLDR01-SV; 1600 ppm H₂O) for H standard and a synthesized CaO-MgO-SiO₂(-C-N) glass for N, C, and Si standard (600 ppm N, 4500 ppm C, and 23.5 weight % Si). Instrumental mass discriminations were 330‰ for the D/H ratio and 5‰ for $^{15}\text{N}/^{14}\text{N}$ ratios. N concentrations ([N]) were calculated from the CC⁻ and the CN⁻ intensities, assuming that [N] is proportional to $I_{\text{CN}} \times I_{\text{CC}}^{-1/2}$. Under these conditions, intensities of $\sim 10^5$ counts/s were obtained for H⁻ and CN⁻ peaks, which allowed reproducibility for δD and $\delta^{15}\text{N}$ to reach ± 60 and $\pm 6\text{‰}$, respectively, with a depth resolution of 10 to 20 nm.
18. The full data set is available at Science Online (www.sciencemag.org/feature/data/1054591.shl).
19. Terrestrial standards having N concentrations of

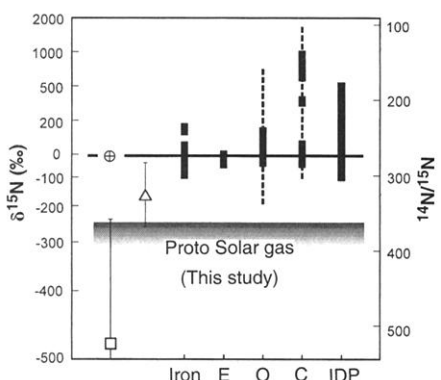


Fig. 3. Comparison of literature $\delta^{15}\text{N}$ values for Earth, meteorites, IDPs, and recently obtained remote-sensing data with the solar value (-240‰ or lower) obtained by this study. The terrestrial range (35) is plotted in a bar with Earth's symbol (\oplus). The open square represents the $\delta^{15}\text{N}$ value for the ammonia in Jupiter's atmosphere (29), whereas the open triangle represents the value for dust from comet Halley (36). The SW data observed by SOHO (28), which are not compatible with our estimate, are not included here. Iron, E, O, and C denote iron meteorites (4), enstatite chondrites (2), ordinary chondrites (3, 6), and carbonaceous chondrites (1, 5), respectively. Solid bars represent mean $\delta^{15}\text{N}$ values for bulk samples, and dotted lines represent $\delta^{15}\text{N}$ ranges observed in stepwise analyses of samples (i.e., $\delta^{15}\text{N}$ values for major N constituents coexisting in them). The $\delta^{15}\text{N}$ values for IDPs range from -100 to +500‰, whereas a major population exhibits enrichments of ^{15}N associated with D-rich hydrogen with δD values up to 25,000‰ (7).

<100 ppm show an almost constant N abundance signature, irrespective of the concentrations, with $\delta^{15}\text{N} \approx -15 \pm 15\%$. There are two major sources for the analytical blank: outgassing of the sample chamber and sample surface contamination. Only the outgassing N is corrected here. This correction represents <1% of the N concentrations and only a few % of the extreme $\delta^{15}\text{N}$ values measured in the first few tens of nm of the grains. At >150-nm depth of the grain, blank (outgassing) N often accounts for ~50% of the detected N, although the exact fraction varies, depending on the analytical condition, such as the sputtering rate or the rastering size. (For the correction for the outgassing N, we adopt the minimum amount among the possible range to avoid overcorrection of the blank.) Degrees of surface contamination are largely variable, depending on grains. The surface contamination is observed prominently at <50-nm depth. Its concentration at the most surface of the sample (when the primary ion beam crosses the border of the gold film and the sample) normally ranges from 100 to 5000 ppm. No systematic difference is observed in the contamination level between the grains in samples 71501 and 79035 or between ilmenite and silicate grains.

20. The δD values of sample 71501 corrected for cosmogenic D ($\delta\text{D}_{\text{trapped}}$), assuming a maximum exposure age of 200 Ma (71) and using a D production rate [L. Merlivat, M. Lelu, G. Nief, E. Roth, *Proc. Lunar Sci. Conf. VII*, 649 (1974)], are available at *Science Online* (18). The amount of cosmogenic D relative to implanted H in grain 1 from sample 79035 is negligible.
21. The best estimate for the minimum $\delta^{15}\text{N}$ value observed in grain 1 from sample 79035 ($-240 \pm 25\%$) is obtained from the weighted average, taken from $\delta^{15}\text{N}$ values as low as -200% . Though lower values are observed, e.g., $-290 \pm 100\%$ (18) at 120-nm depth (Fig. 1A), the differences from the best estimate value are not significant. The observed $\delta^{15}\text{N}$ value (-240%) can be regarded as the upper limit for the SW $\delta^{15}\text{N}$ value, because the observed values are not perfectly free of blank N, especially the surface contamination N.
22. R. Wieler, H. Baur, *Astrophys. J.* **453**, 987 (1995).
23. L. P. Keller, D. S. McKay, *Geochim. Cosmochim. Acta* **61**, 2331 (1997).
24. J.-P. Benkert, H. Baur, P. Signer, R. Wieler, *J. Geophys. Res.* **98**, 13147 (1993).
25. P. Bochsler, R. Kallenbach, *Meteoritics* **29**, 653 (1994).
26. F. Humbert, thesis, Université Henri Poincaré, Nancy 1, France (1998).
27. J. Geiss, G. Gloeckler, R. von Steiger, *Philos. Trans. R. Soc. London A* **349**, 213 (1994).
28. R. Kallenbach et al., *Astrophys. J.* **507**, L185 (1998).
29. T. Fouchet et al., *Icarus* **143**, 223 (2000).
30. E. Zinner, *Annu. Rev. Earth Planet. Sci.* **26**, 147 (1998).
31. M. B. McElroy, Y. L. Yung, A. O. Nier, *Science* **194**, 70 (1976).
32. Assuming that N is lost from a N-bearing host phase with a rate proportional to the inverse square root of the atomic mass ($m^{-1/2}$), 4.5 or 18 orders of magnitude depletion of N concentration is required to enrich ^{15}N by 40 or 300%, respectively, from the initial isotopic composition. To explain by such fractionation the N isotopic composition of CI chondrites, which is enriched in ^{15}N by 40% relative to the solar value, the initial N concentration must be about three orders of magnitude overabundant in comparison to the solar composition (because the N/major solid elements ratio in CI chondrites is 1.7 orders of magnitude lower than the solar value), which is highly unrealistic.
33. N. G. Adams, D. Smith, *Astrophys. J.* **247**, L123 (1981).
34. Ratios averaged over wide depth ranges, rather than H and N isotopic compositions observed at respective depths, are plotted in Fig. 2. This is because the latter may not always reflect the original mixing proportion of the SW and nonsolar components when they were acquired, because H in the present grain is not located at the original site but is diffused over a long range within the grains.
35. B. Marty, L. Zimmermann, *Geochim. Cosmochim. Acta* **63**, 3619 (1999).

36. D. C. Jewitt, H. E. Matthews, T. Owen, R. Meier, *Science* **278**, 90 (1997).
37. Samples were provided by NASA. We thank R. Wieler for constructive comments and suggestions, H. Fukui and O. Ohtaka for preparing the synthetic glass standards, and N. Shimobayashi and M. Kitamura for nondestructive elemental mapping of lunar grains. K.H. thanks members of CRPG-CNRS for their hospitality during his stay. This study was supported by

the Japanese Ministry of Education, Science, Sports and Culture and by CNRS through a "Poste Rouge" fellowship by grants from Institut National des Sciences de l'Univers-Programme, National de Planétologie and from Région Lorraine (K.H.). This work is CRPG-CNRS contribution 1488.

3 August 2000; accepted 29 September 2000

Decadal Sea Surface Temperature Variability in the Subtropical South Pacific from 1726 to 1997 A.D.

Braddock K. Linsley,¹ Gerard M. Wellington,² Daniel P. Schrag³

We present a 271-year record of Sr/Ca variability in a coral from Rarotonga in the South Pacific gyre. Calibration with monthly sea surface temperature (SST) from satellite and ship measurements made in a grid measuring 1° by 1° over the period from 1981 to 1997 indicates that this Sr/Ca record is an excellent proxy for SST. Comparison with SST from ship measurements made since 1950 in a grid measuring 5° by 5° also shows that the Sr/Ca data accurately record decadal changes in SST. The entire Sr/Ca record back to 1726 shows a distinct pattern of decadal variability, with repeated decadal and interdecadal SST regime shifts greater than 0.75°C . Comparison with decadal climate variability in the North Pacific, as represented by the Pacific Decadal Oscillation index (1900–1997), indicates that several of the largest decadal-scale SST variations at Rarotonga are coherent with SST regime shifts in the North Pacific. This hemispheric symmetry suggests that tropical forcing may be an important factor in at least some of the decadal variability observed in the Pacific Ocean.

It is now recognized that significant tropical and subtropical Pacific ocean-atmosphere variability occurs on decadal-to-interdecadal time scales. However, in order to evaluate decadal-scale climate variability over time, climate records long enough to capture multiple decadal periods are needed, and these records are limited (1, 2). In the North Pacific, sufficient instrumental climatic data exist to identify a pattern of irregular decadal-to-interdecadal ocean-atmosphere climate variability over the past ~100 years (2–7). The time history of the leading eigenvector of North Pacific SST back to 1900 A.D. has been termed the Pacific Decadal Oscillation (PDO) by Mantua et al., (6). The PDO is a recurring pattern of ocean-atmosphere variability in which the central gyre cools at the same time as the eastern margin warms, or vice versa. Alternating phases of the PDO can last for two to three decades, with reversals being noted in 1924/25, 1946/47, and 1976/77 (6). Before 1900, little is known about decadal variability in the North Pacific. In the

South Pacific, oceanographic data are extremely sparse. However, the limited data indicate that the subtropical South Pacific may also play a role in decadal-scale oceanographic variability in the Pacific (8–11). For example, the South Pacific is currently the dominant (50 to 75%) source region for isopycnal water transport to the equatorial thermocline (10, 11). This is due in part to the partial blocking effect of the surface ocean beneath the Intertropical Convergence Zone (ITCZ) in the North Pacific and the more limited influence of the South Pacific Convergence Zone (SPCZ) on South Pacific isopycnal equatorward flow (8, 11).

The spatial pattern of decadal variability in Pacific SSTs is similar to that associated with El Niño–Southern Oscillation (ENSO), but with lower amplitude in the tropics and higher amplitude outside the tropics (3, 12). Some studies suggest that this decadal variability may originate in the subtropics of the North Pacific Ocean through unstable ocean-atmosphere interactions (2, 13), whereas other studies suggest that tropical ENSO forcing plays a key role (3, 12, 14, 15). However, several key questions regarding the nature of Pacific decadal variability remain, including the recurrence period of decadal changes in SST; whether the decadal-scale SST variability in the subtropical South Pacific is in phase with the North Pacific; and

¹Department of Earth and Atmospheric Sciences, ES 351, University at Albany–State University of New York, Albany, NY 12222, USA. ²Department of Biology and Biochemistry, University of Houston, Houston, TX 77204, USA. ³Laboratory for Geochemical Oceanography, Department of Earth and Planetary Sciences, Harvard University, Cambridge, MA 02138, USA.